The Dynamics of a Polygon in a Swirling System

Guanhau Sun
Mentor: Prof. Miranda Holmes-Cerfon

10/2019

Abstract

In this project, we continue to study a previously discovered phenomenon that granular material in a swirled container can have different dynamical behaviors based on its density in the container. Here we reduce the granular system to a single polygon whose geometry and size can vary. We investigate the relationship between its dynamical behavior and its size, geometry, friction in the system and the swirling motion. Both numerical simulations and experiments are conducted. So far we have reaffirmed that friction in the system plays an important role.

Part I

Introduction

Granular material in a swirling environment attains many fascinating behaviors both with or without fluids. Many of them have been surveyed in [1]. In particular, we are interested a simple, yet amazing phenomenon described in [2],[3]about marbles' dynamics in a swirling system. The phenomenon is that marbles in a swirling system can rotate or counter-rote, compared to the direction of the swirling motion, based on their density in the system. Lee et al.(2019) suggest that the friction in the system enforce the formation of a rigid raft when the density is high enough and the no-slip condition between the rigid raft and the swirling boundary, and counter-rotation becomes a direct product. However, the dynamics of such a rigid raft in the swirling medium was unknown, and the role of friction was only observed but not further understood. We wish to understand friction less from a mechanical, but more from a statistical point of view from its influences to our system. On the basis of that, we may regain knowledge on how the mechanic works , and even mimic the role of friction with other operations.

Part II

Model

1 Basic Setting

In previous studies, the granular medium is usually held nearly on a plane: there's no specific indication that vertical movement plays a role in the system. Therefore, we will deal with a 2D model. As shown in Figure 1, the polygon, in this case, is a regular hexagon with radius R_p, positioned in a circular container with radius R_c, which is swirling around a static center with radius r_s and angular velocity ω_s . If the container keeps swirling, the polygon inside will keep colliding with the boundary, and the dynamic behaviors of the polygon is our object to study. Notably the container itself is not rotating,

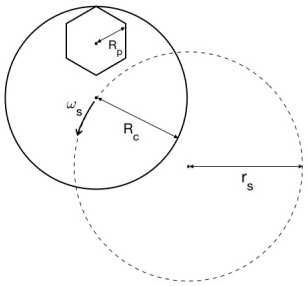

Figure 1: The basic geometric setting of the problem. Symbols are described in Table 1

Parameter	Symbol	Typical Range	Unit
Radius of the Circular Container	R_c	7	
Radius of the Regualr Polygon	R_p	0.7-6.5	
Sides of the Polygon	N	3(Triangle) -∞(Disk)	
Amplitude of the Swirling	r_s	1 - 10	
Angular Velocity of the Swirling	ω_s	1 - 10	
Friction Coefficient	μ	0 - 1	
Restitution Coeficient	e	0.9 - 1	
Mass of the Polygon	m_p	1	
Mass of the Container	∞		
$\frac{R_p}{R_c}$	α	0.1-0.9	-
$\frac{r_s}{R_c}$	β	0.1-5	-

Table 1: The basic parameters

but only translating in a circular path. Now we introduce all the parameters and their ranges that will be used in the simulation and experiment in Table 1.

Among these parameters, we can define a few useful dimensionless quantities. We will define

$$\alpha = \frac{R_p}{R_c}$$

that represents the relative size of the polygon compared to the circular boundary, and

$$\beta = \frac{r_s}{R_c}$$

that represents the relative size of the swirling motion, compared to the radius of the container. α and β describe the geometry of the system.

2 Rigid Body Dynamics

The whole system is governed by rigid body dynamics when not in collisions because the ground friction is ignored. Because the polygon is convex and only its vertex can hit the boundary, we will discretize the polygon by its vertex, whose position is represented by $X_i(t)$ and i is the index of the

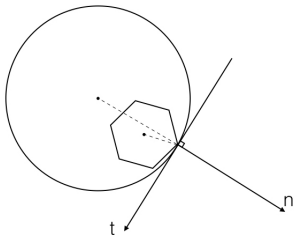

Figure 2: The figure shows a collision between a hexagon and the circular boundary. The normal and tangential directions are well-defined based on the circular geometry.

vertices. $X_{cm}(t)$ will represent polygon's geometric center, which is also the center of mass in our case; $\tilde{X}_i$ represents the relative position of each vertex to the center, defined as $\tilde{X}_i = X_i - X_{cm}$; $R(t)$ is the rotational matrix that decides the relative positions of the vertex to the center of mass, and $O(t)$ represents the center of the circular container, controlled by the swirling motion. All together, the system starts with $X_0, v_p, \omega_p, \omega_s$ is governed by the following equations:

$$\begin{aligned} X_i(t) &= X_{cm}(t) + \tilde{X}_i(t) \\ X_{cm}(t) &= X_0 + v_p t \\ \tilde{X}(t) &= R(t) \cdot \tilde{X}_0 \\ R(t) &= \begin{pmatrix} \cos(\omega_p t) & -\sin(\omega_p t) \\ \sin(\omega_p t) & \cos(\omega_p t) \end{pmatrix} \\ O(t) &= r_s(\cos(\omega_s t), \sin(\omega_s t)) \end{aligned}$$

We will not discretize the container's boundary because the simulation method we are adopting, which will be described later in Part III.

3 Collision Law

The key part in the swirling system is the collision between the polygon inside and the boundary. Rigid body collisions with friction. In this paper we adopt the results provided by Mason and Wang(1992). Following are core postulations:

1. The rigid body will collide only at a point.
2. The collision process is instantaneous, i.e no displacements occur during the Colin, and linear and angular velocities of the bodies have discontinuous changes.
3. Interactive forces are impulsive, and all other finite forces are negligible.

To further explain the collision process, figure(2) shows a collision between two bodies and the contact point is taken as the origin, which is guaranteed by our first assumption. We know $m_i, v_i, I_i, \omega_i (i = 1, 2)$, which are the corresponding mass, incoming velocity, moment of inertia and angular velocity of body 1 or body 2. Also, the position X_i and center of mass X_i^{cm} for each body is known. Due to the second and third assumption, all we need to update through the collision are v_i and ω_i. This calculation will be done in the impulse space, where the impulse is defined to be the change of momentum of the body as

$$P_i = \lim_{\tau \to 0} \int_0^\tau F_i \, dt$$

This definition is attained by imagining the collision process to last from time 0 to τ, and the change of momentum is the integral of the force, defined to be finite.

By using the above definition of impulse we derive two master equations:

$$m_i(V_i - v_i) = (-1)^i P \tag{1}$$

$$I_i(\Omega_i - \omega_i) = (-1)^i P \times r_i \tag{2}$$

where capital letter V_i, Ω_i denote the terminal velocities we want to solve, and lower case v_i, ω_i are the incoming velocities that we know.

The next step is to find the tangent and normal directions for decomposition. In our case, though the polygon is pointy, because the outer boundary is circular, the tangent and normal directions are well defined at any point. We will decompose $P = P_n \cdot \hat{n} + P_t \cdot \hat{t}$, and we can compute P_n and P_t separately to decide the total impulse. In normal direction, coefficient of restitution e deicides how elastic the collision is: $e = 1$ represent perfectly elastic collision, while $e = 0$ represents perfectly inelastic collision. In tangential direction, Friction will be coulomb friction:

$$f = -s\mu N$$

where μ is the friction coefficient, N is the normal force, and s is the sign of the slipping velocity, making the friction to be a counterforce of the motion. If we write out (1) and (2) in components, we will have 3 equations and 5 unknowns(in 2D). The last two equations will be brought in either by Newton's or Poisson's hypothesis, both presenting the relationship between the normal impulse and the tangential impulse.

Newton's hypothesis The formulas for P_n and P_t that are used in our simulation and other details are provided in the appendix.

Part III
Simulation

4 Event-Driven Method

We adopt an event-driven simulation for the model, in which each collision is solved numerically based on the exact rigid body motion equations that we previously described. To solve the collision, we must solve the master equation

$$\parallel X_i(t_i) - O(t) \parallel = R_c$$

for each i. Each solution represents the corresponding vertex touches the boundary. Then we take the smallest t_i, which represents the first collision, as t_c to be the real time for next collision to happen. To conclude, our simulation algorithm works as follows:

Step1: Solve the master equation to find the next collision.

Step2: Update the position and velocity up to the point just before the collision.

Step3: Update the velocity by our collision laws.

Step4: Repeat

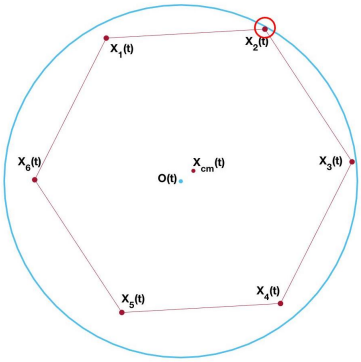

Figure 3: This plot shows the hexagon colliding to the boundary at the second vertex.

To initiate the simulation, we will give the polygon a random velocity of norm 1 to start the above algorithm.

Step one will involve solving the master equation, which requires to solve a 2 by 2 nonlinear system. In this case we adopt a combination of bisection and Newton method to solve it, the details are given in the appendix. Notably, because the numerical solver doesn't know physics, we have to check if a solution is physical. Besides being the numerical solution of our master equation, for every solution we will check:

1. 1. If the relative normal velocity of the vertex to the tangent plane is pointing outward.
2. 2. If all the points are staying in the container. The first check tells us if the point hits the boundary from outside or inside; the second check tells us if all points are in the container when the collision happens.

If any check fails, it means our solver returns an incorrect solution or a correct solution which is not the smallest. Some geometric methods are also introduced in this process, and also described in the appendix.

Step two will use the rigid body dynamics equations described in section 2. In particular, instead of solving exactly

$$\parallel X_i(t_i) - O(t) \parallel = R_c$$

we will solve

$$R_c - \parallel X_i(t_i) - O(t) \parallel - R_c < \epsilon$$

where ϵ is the tolerance of error by our choice. In the following simulations, $\epsilon = 10^{-13}$. Finally, step three will use the formulas we provide in section 3.

5 Results

To characterize the dynamical behavior of the polygon, we will look at the trajectory of the center of mass(X_{cm}) and the velocity of the center of mass(v_{cm}) from a dynamic system perspective, and the angular velocity(ω_p) and energy of the polygon($E_p = \frac{1}{2}mv_p^2 + \frac{1}{2}I\omega_p^2$) from a more mechanical point of view. We can define one more dimensionless quantity:

$$S = \frac{\omega_p}{\omega_s},$$

which compared the angular velocity of the polygon to the swirling motion. In the simulations, we will investigate how $\alpha = \frac{R_p}{R_c}$,$\beta = \frac{r_s}{R_c}$ and μ influence the dynamical and mechanical behavior of the polygon.

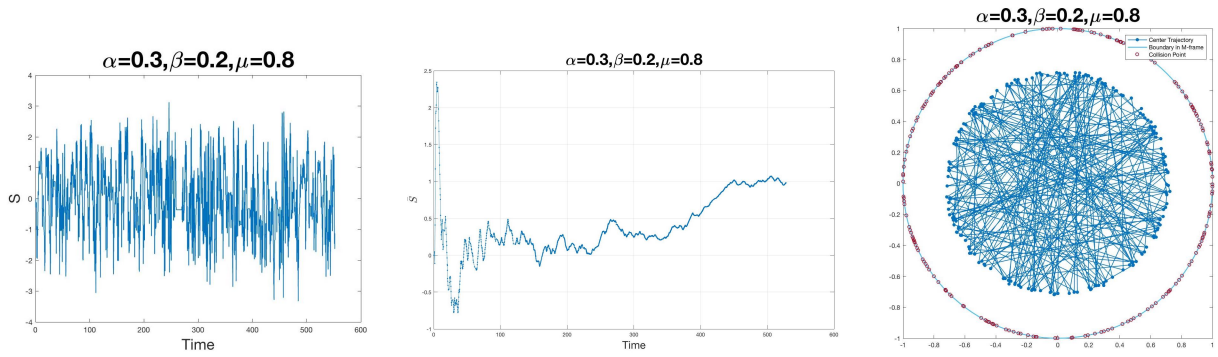

(a) (b) (c)

Figure 4: Chaotic mode:In fig(a), we are showing the S/Time plot; fig(b) is the time average of fig(a); fig(c) records the collision in the M-frame.

For now, we conduct 50 simulations for one set of parameters, and each simulation will contain 2000-4000 collisions in order to observe the average dynamic behaviors. The collisions are perfectly elastic ($e = 1$).

5.1 Dynamic Modes

In simulations, we observe that the polygon has generally three dynamic modes: Chaotic, Periodic and Stable. To quantify the chaotic degree of the system, we will measure the distance between two points in the time-rotation$(t - S)$ map by the binary function:

$$D_\delta(i,j) = \begin{cases} 1 & if \parallel x(i) - x(j) \parallel \leq \delta \\ 0 & otherwise \end{cases}$$

where δ is our tolerance to define what does it mean to be "same." Then we will calculate the recurrence rate RC by

$$RC = \frac{1}{N^2} \sum_{i,j=1}^{N} D_\delta(i,j)$$

where N is the number of points we have in one simulation. If all the points have the same position, $RC = 1$; if half of them appear at one position and the other half at another position, $RC = 1/4$. This will help us measure how chaotic the system is. Notably, because the recurrence rate drops fast, to minimize the influence of the transient, we will take average or use other simplifications that will be specified in the case.

5.1.1 Chaotic

Figure 4(a) shows a typical time-rotation plot of a chaotic rotating polygon. No pattern is usually observed in the span of 2000-4000 collisions and the trajectory of center of mass tends to cover the whole circular area. We are viewing the trajectory of center of mass in the M-frame(rotational) frame instead of the lab frame in figure 4(c). The recurrence rate in the chaotic mode is nearly $0(RC < 10^{-4})$ and the time average plot of the rotation also has no tendency to converge.

5.1.2 Quasi-Steady

In some cases, a periodic rotation pattern is observed: after a certain number of collisions, polygon settles down to 2 or more modes that it tends to follow. Figure 5 shows such periodic pattern.

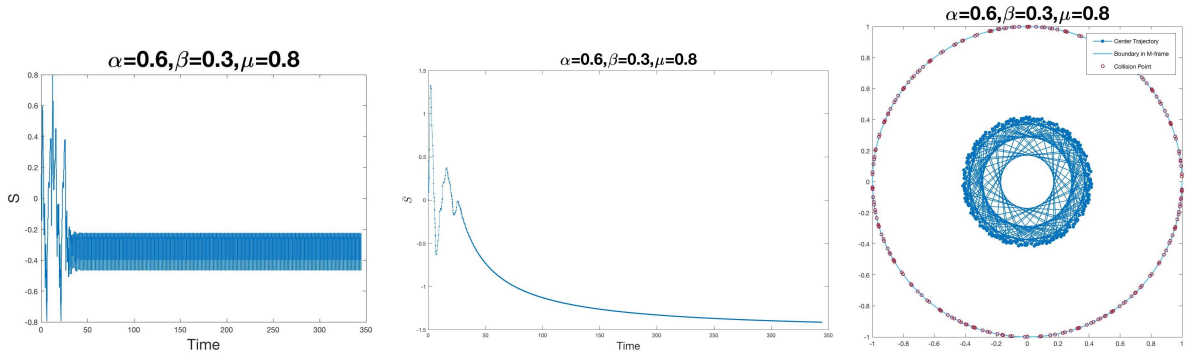

(a) (b) (c)

Figure 5: Quasi-Steady mode: three plots are corresponding to ones shown in the chaotic mode. Particularly, we can observe three concentric circles in the center of fig(c), which are the corresponding tangential circles for three modes in the limit cycle in the quasi-steady model.

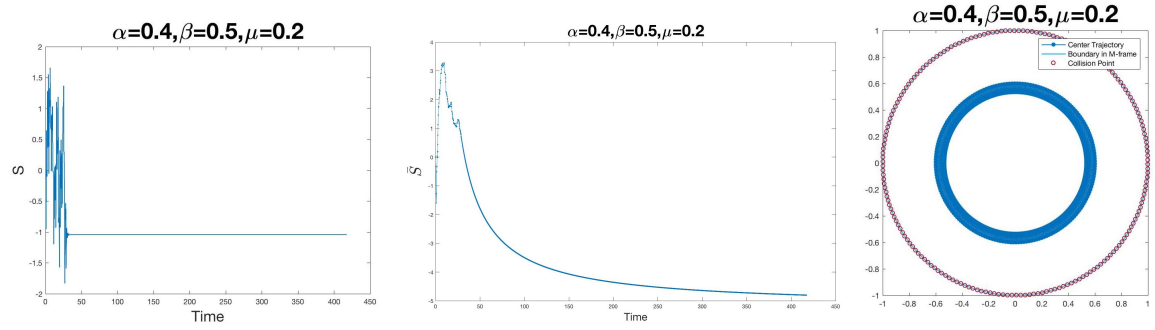

(a) (b) (c)

Figure 6: Steady mode: three plots are the same as mentioned before. Now in fig(c), we only observe one tangential circle of the trajectory.

5.1.3 Steady

Finally, we observe polygons can settle down just to one angular velocity, making the energy also constant. The trajectory of mass center tends to fill up the annulus regularly, meaning the collision is happening linearly in time. Figure 6 shows those behaviors.

5.2 Friction

Friction was thought to be critical in producing the counter-rotation phenomenon in (Lee&Ryan, PRE 2019), in our simulations, we observe the similar phenomenon: When $\mu = 0$, average positive rotation is generally observed; When $\mu \neq 0$, counter-rotation is generally observed. Surprisingly, once we have friction in the system, its magnitude hardly plays any role in the system as we can see from Figure 7, where β is fixed to be 0.1. Similar phenomenon is observed for all range of β.

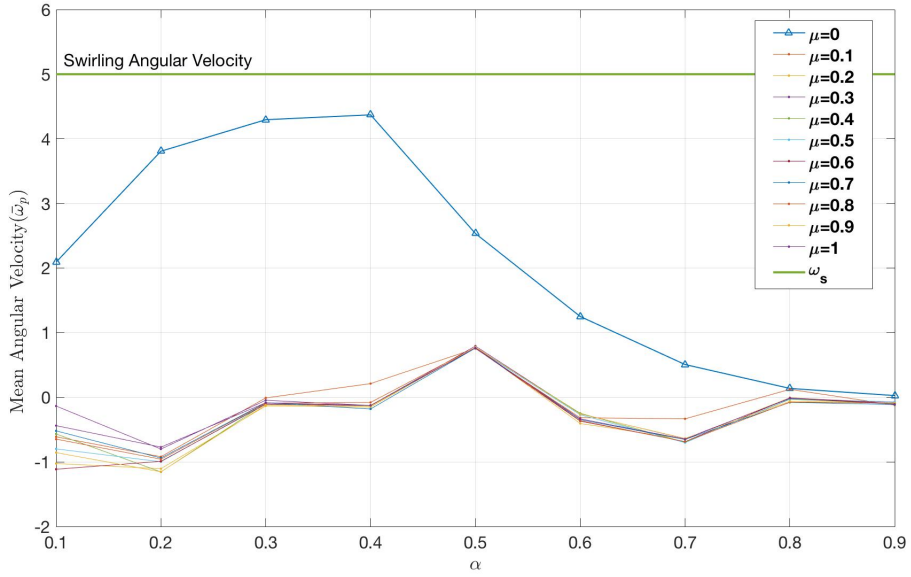

Figure 7: This figure when $\beta = 0.1$, instead of having S on the axis, compares the swirling angular velocity directly with the real mean angular velocity of the polygon. We observe that there's qualitative difference between $\mu = 0$ and $\mu \neq 0$.

Part IV
Discussion and Future Works

So far, we reaffirm that friction is critical for the polygon to counter rotate. We also found the interesting phenomenon that, however, the magnitude of the friction does not matter. We also found that the dynamical behavior of the polygon is largely correlated to its mechanical behavior, i.e the trajectory of the mass center settles down when the rotation of the body settles down. In the future, we would like to explain those phenomenons. Moreover, there're many parameters in the system that we haven't investigated: geometry of coefficient of restitution. They are expected also to play important roles as well: does it make a difference if the polygon is a triangle, hexagon or octagon?

On the other hand, our assumptions for the rigid body collisions are never tested. We plan to do an experimental study from this perspective in the near future as well.

Part V
Appendix

Collision Laws

In this part we will introduce the method provided by Wang and Mason, which is an extension Routh's method introduced in 1924. They provided the formulas for both Newton and Poisson's hypothesis, without giving the details of the calculation, which will be provided here. Also some typos in their paper will be noted.

by defining the collision happens from time 0 to τ and force F is from body 1 to body 2. Now we write eqn 1- 2 in components for each body:

$$m_1(V_{1n} - v_{1n}) = -P_n \tag{3}$$
$$m_2(V_{2n} - v_{2n}) = P_n \tag{4}$$
$$m_1(V_{1t} - v_{1t}) = -P_t \tag{5}$$
$$m_2(V_{2t} - v_{2t}) = P_t \tag{6}$$
$$I_1(\Omega_1 - \omega_1) = -P \times r_1 \tag{7}$$
$$I_2(\Omega_2 - \omega_2) = P \times r_2 \tag{8}$$

the subscript t, n means the tangential or normal direction.

Now we use the friction law, which says $F_\mu = -sgn(v_t)\mu * |F_n|$. If we integrate both sides from 0 to τ, we know $P_t = s\mu|P_n|$ with a sign s to decide. This tells us that

$$P = P_n * \hat{n} + P_t * \hat{t} = P_n(\hat{n} + \mu\hat{t}) \tag{9}$$

So all we need to do is to decide P_n in (9) and substitute it back to (3)-(8) to update all the quantities. Here we use Newton hypothesis, stating the following relation about the normal component of the terminal and initial relative velocity:

$$V_{rn} - v_{rn} = -(1 + e)v_{rn} \tag{10}$$

where $e \in [0, 1]$ is the coefficient of restitution. When $e = 0$, the collision is pure inelastic; when $e = 1$, the collision is pure elastic. And $V_{rn}, v_{rn}$are the normal components of the relative velocity, which are

$$V_{rn} = V_r * \hat{n} = [(V_1 - \Omega_1 \times r_1) - (V_2 - \Omega_2 \times r_2)] * \hat{n}$$
$$v_{rn} = v_r * \hat{n} = [(v_1 - \omega_1 \times r_1) - (v_2 - \omega_2 \times r_2)] * \hat{n}$$

We first calculate the cross products on the side:

$$\omega_i \times r_i = \begin{vmatrix} \hat{t} & \hat{n} & \hat{z} \\ 0 & 0 & \omega_i \\ r_{it} & r_{in} & 0 \end{vmatrix} = -r_{in}\omega_i * \hat{t} + r_{it}\omega_i * \hat{n}$$

then we are able to write down

$$V_{rn} - v_{rn} = (V_{1n} - v_{1n}) - r_{1t}(\Omega_1 - \omega_1) - (V_{2n} - v_{2n}) + r_{2t}(\Omega_2 - \omega_2) \tag{11}$$

now we can substitute (3)-(8) to (10) and find

$$V_{rn} - v_{rn} = -\frac{P_n}{m_1} + r\frac{P \times r_1}{I_1} - \frac{P_n}{m_2} + r_{2t}\frac{P \times r_2}{I_2}$$

Again we compute the cross product

$$P \times r_i = \begin{vmatrix} \hat{t} & \hat{n} & \hat{z} \\ P_t & P_n & 0 \\ r_{it} & r_{in} & 0 \end{vmatrix} = (P_t r_{in} - P_n r_{it}) * \hat{z}$$

continuing the calculation:

$$V_{rn} - v_{rn} = -\frac{P_n}{m_1} + r_{1t}\frac{P_t r_{1n} - P_n r_{1t}}{I_1} - \frac{P_n}{m_2} + r_{2t}\frac{P_t r_{2n} - P_n r_{2t}}{I_2} \tag{12}$$

now use (9),

$$V_{rn} - v_{rn} = -P_n(\frac{1}{m_1} + \frac{1}{m_2} - r_{1t}\frac{\mu r_{1n} - r_{1t}}{I_1} - r_{2t}\frac{\mu r_{2n} - r_{2t}}{I_2}) = -(1 + e)v_{rn}$$
$$\Rightarrow P_n = (1 + e)v_{rn}q_n \tag{13}$$

where $q_n$is $(\frac{1}{m_1}+\frac{1}{m_2}-r_{1t}\frac{\mu r_{1n}-r_{1t}}{I_1}-r_{2t}\frac{\mu r_{2n}-r_{2t}}{I_2})^{-1}$. Similarly, we can write the change of relative tangential velocity:

$$\begin{aligned} V_{rt}-v_{rt} &= -\frac{P_t}{m_1}-r_{1n}\frac{P_t r_{1n}-P_n r_{1t}}{I_1}-\frac{P_t}{m_2}-r_{2n}\frac{P_t r_{2n}-P_n r_{2t}}{I_2} \\ &= -(\frac{1}{m_1}+\frac{1}{m_2}+\frac{r_{1n}^2}{I_1}+\frac{r_{2n}^2}{I_2})P_t-(\frac{r_{1n}r_{1t}}{I_1}-\frac{r_{2n}r_{2t}}{I_2})P_n \end{aligned}$$

So now we fully solve (3)-(8):

$$\begin{aligned} V_{in}-v_{in} &= (-1)^i(1+e)v_{rn}q_n/m_i \\ V_{it}-v_{it} &= (-1)^i\mu(1+e)v_{rn}q_n/m_i \\ \Omega_i-\omega_i &= (-1)^i(1+e)(\mu r_{in}-r_{it})v_{rn}q_n/I_i \end{aligned}$$

However, this calculation is only valid in a few cases. The core of the calculation is (eqn 10), which gives the relationship between the terminal and incoming velocity. Under such hypothesis, it is known that the above calculation may give energy gain in many cases(Kane, 1984; Keller, 1986). The other choice is to adopt Poisson's hypothesis, which divides the collision process into two phases: compressive phase, which describes the process until the normal velocity decays to zero, and restitution phase that describes the process for normal velocity to recover from zero. The total normal impulse is defined to be the sum of the impulses from those two phases:

$$P_y = P_r + P_C$$

Poisson's hypothesis gives the relation

$$\frac{P_r}{P_c} = e$$

We will later compare the results attained by adopting different hypothesis. The following collision formulas(Wang and Mason) for different contact modes will be used in the simulation. Please see here: `https://modelingsimulation.github.io/undergraduateClass/`

Numerical Solver

As said in section 4, the equation we want to solve is

$$R_c - \parallel X_i(t_i) - O(t) \parallel < \epsilon$$

We can write $X_i(t_i) - O(t)$ explicitly

$$\begin{aligned} X_i(t) - O(t) &= X_{cm}(t) + \tilde{X}_i(t) - O(t) = X_{cm}(t) + R(t)\cdot\tilde{X}_0 - O(t) \\ &= \begin{pmatrix} X_{cm}^\alpha \\ X_{cm}^\beta \end{pmatrix} + \begin{pmatrix} \cos(\omega_p t) & -\sin(\omega_p t) \\ \sin(\omega_p t) & \cos(\omega_p t) \end{pmatrix} \begin{pmatrix} \tilde{X}_0^\alpha \\ \tilde{X}_0^\beta \end{pmatrix} - r_s \begin{pmatrix} \cos(\omega_s t) \\ \sin(\omega_s t) \end{pmatrix} \\ &= \begin{pmatrix} X_{cm}^\alpha - r_s\cos(\omega_s t) + \tilde{X}_0^\alpha\cos(\omega_p t) - \tilde{X}_0^\beta\sin(\omega_p t)] \\ X_{cm}^\beta - r_s\sin(\omega_s t) + \tilde{X}_0^\alpha\sin(\omega_p t)] + \tilde{X}_0^\beta\cos(\omega_p t)] \end{pmatrix} \end{aligned}$$

and we observe this is a non-linear system to solve. Our method is two-fold: first, we use some geometric methods to calculate the lower and upper bounds for our solution by solving a set of quadratic equations; then we use bisection and Newton methods to find the more accurate solution in different intervals.

We will illustrate our geometric methods in the case of a triangle. Because the polygon is convex and regular, before the polygon hits the circular boundary, its out-scribed circle must hit the boundary (illustrated in Figure8(a)); And when two points of a polygon touches, the distance between the center

of polygon and the boundary reaches its minimum. So we can calculate those two times to be the lower and upper limit of our guesses. And they are solutions of the quadratic equations

$$\begin{cases} \| X_{cm}(t_o) \| = & 1 - r_p \\ \| X_{cm}(t_i) \| = & 1 - r_b \end{cases}$$

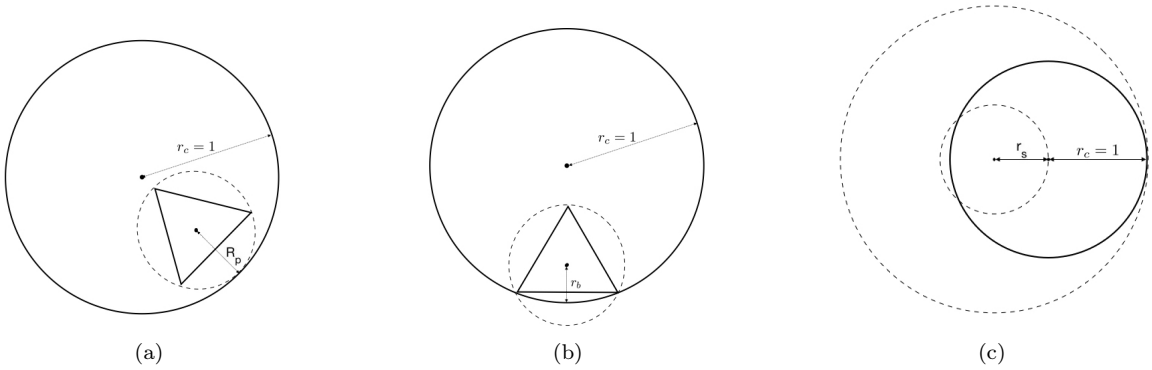

(a) (b) (c)

Figure 8: We demonstrate three situations that are considered in finding reasonable guesses for our numeric solver: fig(a) shows when the outscribed circle hits the boundary, while the triangle has not; fig(b) shows the situation when; fig(c) shows the swirling trajectory and the outer circle that the container can reach.

where r_b is the distance between the center of polygon to the boundary, which can be calculated analytically.

Moreover, when the outer boundary is swirling, the points on the boundary can form a larger circular loop, whose radius is $1+r_s$ and a smaller loop whose radius is $1-r_s$. Then we will adopt the previous method to the larger loop and smaller loop, giving us four guesses in the order of $0 < t_{ib} < t_{ob} < t_{is} < t_{os}$.

After getting initial guesses for the solution, we will start bisection in each interval between the four guesses and zero. To ensure we get the smallest solution, our bisection method will always choose the smaller interval, when facing two solutions in the current interval. After 8-10 times of bisection, we are pretty confident that Newton method will converge fast enough and will give us the final solution. Then the solutions will go through the check described in Section 4 and give us the right one.

References

[1] Lisa M. Lee, John Paul Ryan, Yoav Lahini, Miranda Holmes-Cerfon, and Shmuel M. Rubinstein Phys. Rev. E 100, 012903 (2019)

[2] M. A. Scherer, V. Buchholtz, T. Pöschel, and I. Rehberg, Phys. Rev. E 54, 4560(R) (1996).

[3] Michael A. Scherer, Karsten Kötter, Mario Markus, Eric Goles, and Ingo Rehberg Phys. Rev. E 61, 4069 (2000)

[4] Y. Wang and M. T. Mason, J. Appl. Mech. 59, 635 (1992).

[5] Keller, J. B., "Impact with Friction," ASME JOURNAL OF APPLIED MECHANICS, Vol. 53, pp. 1-4 (1986).

[6] Kane, T. R., "A Dynamics Puzzle," Stanford Mechanics Alumni Club Newsletter, p. 6 (1984)